Journal of Power Sources 196 (2011) 2221–2226

Contents lists available at ScienceDirect

Journal of Power Sources

journal homepage: www.elsevier.com/locate/jpowsour

Precipitated nanosized titanium dioxide for electrochemical applications

S.A. Kirillov[a,b,*], T.V. Lisnycha[b], S.I. Chernukhin[a]

[a] Joint Department of Electrochemical Energy Systems, 38A Vernadsky Ave., 03142 Kyiv, Ukraine
[b] Institute for Sorption and Problems of Endoecology, 13 Gen. Naumov St., 03164 Kyiv, Ukraine

ARTICLE INFO

Article history:
Received 2 July 2010
Received in revised form 8 September 2010
Accepted 21 September 2010
Available online 29 September 2010

Keywords:
Lithium batteries
Anode materials
Titanium dioxide
Crystalline
Amorphous

ABSTRACT

Two types of titanium dioxide samples precipitated from aqueous solutions of titanium tetrachloride are investigated. Crystalline materials are obtained by means of neutralization of $TiCl_4$ with the solution of an alkali metal hydroxide. The change of the order of mixing leads to amorphous materials. The evolution of the samples upon the thermal treatment is characterized using XRD, SEM, TEM and porosity studies. The application of crystalline TiO_2 as an electrode material in lithium-ion 2016 sample cells enable one to yield specific currents up to 3350 mA g^{-1}. On the other hand, the thermal treatment of initially amorphous materials does not lead to complete crystallization, and the presence of amorphous TiO_2 is well seen as the so-called capacity behavior of cyclic voltammetry curves.

1. Introduction

Titanium dioxide is widely employed in numerous applications [1], from pigments to bone implants, and its relatively new function is an electrode material for lithium ion batteries. An ability of the anatase modification of TiO_2 to reversibly insert and deinsert lithium ions has been first noticed in 1979 [2] and carefully studied in numerous subsequent papers, see, e.g., Refs. [3–10]. Obvious advantages of this material making it a good alternative to carbonaceous anodes are cheapness, safety and non-toxicity. Lithium insertion in natural and synthetic TiO_2 modifications has been reviewed in Ref. [11].

Among natural TiO_2 polymorphs, anatase is less dense than rutile and brookite (d = 3.84, 4.26 and 4.17 g cm^{-3}, respectively) and most easily accommodates lithium ions. In bulk, rutile is the most thermodynamically stable modification of TiO_2, and the phase stability sequence at ambient temperatures is rutile–brookite-anatase. As shown in calorimetric measurements by Navrotsky and co-workers [12,13], this sequence changes in nanophases. For crystallites of less than ~50 nm size, when the surface area reaches 50 m^2 g^{-1}, anatase becomes more stable than rutile and brookite at ambient temperatures.

Structure relations between anatase and its lithiated relatives have been analyzed in great detail [14,15]. Anatase belongs to distorted spinel structures. Unlike the true cubic spinel (space group $Fd3m$, Z = 4), the tetragonal anatase structure (space group $I4_1/amd$, Z = 4) is elongated in [0 0 1] direction (along the c edge of the unit cell) and can be considered as a stacking of two one-dimensional zigzag chains consisting of distorted edge-sharing TiO_6 octahedra. This stacking is equivalent in [1 0 0] and [0 1 0] directions (the a and b edges of the unit cell) and leads to empty zigzag channels formed by highly distorted octahedral holes.

Filling these holes with lithium ions requires lowering the oxidation number of titanium and gives rise to two possible structures. If a half of free octahedral positions are occupied, a $Li_{0.5}TiO_2$ compound emerges whose symmetry is lowered from $I4_1/amd$ to Imma, Z = 4. In its structure, lithium is statistically distributed over accessible holes. This results in lengthening the a and b edges of the unit cell and shortening the c edge; the unit cell volume increases by ~3.5%.

Further addition of lithium enables one to enrich $Li_{0.5}TiO_2$ with additional cations and approach a $LiTiO_2$ stoichiometry. In the latter compound, all empty positions are filled, and the tetragonal anatase structure $I4_1/amd$ is recovered [15]. The a edge of the unit cell stretches, the b edge remain almost the same, and the c edge shrinks. However, the unit cell volume does not vary. This means that the anatase framework experiences little distortion upon lithium insertion, if compared to the parent structure, since the ionic radii of Ti^{4+}, Ti^{3+} and Li^+ are quite close (0.61, 0.67 and 0.68 Å, respectively).

A plethora of information regarding the insertion process has been accumulated by means of x-ray and neutron studies, Raman spectroscopy, quantum chemistry calculations, etc. (see Refs. [15–18] and references cited therein).

* Corresponding author at: Joint Department of Electrochemical Energy Systems, 38A Vernadsky Ave., 03142 Kyiv, Ukraine. Tel.: +380 44 424 35 72; fax: +380 44 424 62 40.
E-mail address: kir@i.kiev.ua (S.A. Kirillov).

0378-7753/$ – see front matter © 2010 Elsevier B.V. All rights reserved.
doi:10.1016/j.jpowsour.2010.09.049

From the point of view of thermodynamics, based on the reaction of incomplete insertion, which is more common in electrochemical applications:

$$TiO_2 + 0.5e^- + 0.5Li^+ \leftrightarrow Li_{0.5}TiO_2,$$

the theoretical specific capacity of the titanium dioxide (anatase) electrode is 167.5 Ah kg^{-1}. The Li/TiO_2 (anatase) cell presents a stable working voltage plateau of about 1.78 V [2].

Almost all studies of lithium intercalation in anatase have been performed with nanosized materials. It has become common use that subdivision adds evident functionality to electrode applications extending electrode–electrolyte contact area, shortening pathways for both electronic and ionic transport and facilitating lithium insertion, resulting in significant growth of discharge rate (specific power) [19]. These advantages of nanoscale materials have been convincingly confirmed in comparative studies of micro- and nanosized anatase [7,15,20,21]. Most recent researches employ anatase samples of various morphology, like hollow spheres [22,23], nanowires [24] and nanotubes [25–27]. Mesoporous materials are widely investigated [28], including those with prescribed pore distribution obtained by means of templation with block-copolymers [29] or colloidal spheres [30]. Numerous tailored materials have been examined, like solid solutions and composites modified by carbon [20,22,25,31], phosphate [32], copper and tin [33], Al_2O_3 [34], SiO_2 and RuO_2 [27], etc.

All these data refer to materials obtained by means of hydrolysis of organic derivatives of titanium, whereas industry's expectations are bound up with the methods based on approaches prospective to large scale implementation, like spray pyrolysis or hydrolytic precipitation of titanium chloride. It should be noticed that nanosized TiO_2 for lithium batteries produced by spray pyrolysis technology is readily available on the market [35].

In spite of apparent simplicity, hydrolytic precipitation methods performed at carefully controlled conditions can lead to nano-scale materials with extended properties. For example, it has been found in our studies [36–38] that nanosized mesoporous sorbents with extremely high affinity to inorganic cations can be obtained by means of hydrolytic procedures involving titanium chloride. In this paper, samples of titanium dioxide synthesized in a similar way are investigated. It appears that depending on the order of mixing, the samples obtained are either crystalline or amorphous. We report on their characterization and test them as electrode materials in lithium-ion power sources.

2. Experimental

TiO_2 samples were precipitated from solutions of $TiCl_4$ in hydrochloric acid and lithium hydroxide. Precursor I was obtained by means of neutralization of $TiCl_4$ with LiOH; precursor II—by means of adding $TiCl_4$ to LiOH. Precipitates were aged for 24 h, filtered, washed with distilled water until pH 7 was reached, and air-dried.

The properties of samples were studied by means of the following methods. Dehydration, crystallization and/or crystallite growth were investigated using thermal analysis (Q 1500 D, MOM, Hungary) and powder X-ray diffraction (a DRON-4-07 X-ray diffractometer, LOMO, Russia, Cu K_α radiation, Ni filter). Morphology of samples was determined on a JEOL (Japan) JSM 6100 scanning electron microscope and a JEM 200A transmission electron microscope. Measurements of surface areas and pore volumes, and calculations of pore size distributions in terms of the Barrett–Joiner–Halenda method were made on a Micromeritics (USA) ASAP 2000 instrument (nitrogen adsorption–desorption isotherms at 77 K).

Electrochemical studies were performed in two-electrode 2016 coin cells with lithium metal serving as a counter and reference electrode on a home-made versatile electrochemical workstation using cyclic voltammetry and galvanostatic charge/discharge cycling methods. Working electrodes were prepared as follows. TiO_2 powder, graphite (KS6), and a binder (poly(vinylidene difluoride)) were mixed in a weight ratio of 85:10:5 and blended in several drops of *N*-methylpyrrolidone. The mixture was cast onto a 20 μm thick copper foil using a laboratory doctor blade, and cut. The amount of TiO_2 in the electrode material varied from 10 to 15 mg cm^{-2}. The experimental cells were assembled in a glove box filled with high-purity argon (H_2O content less than 1 ppm). A 1 mol L^{-1} solution of $LiClO_4$ dissolved in a mixture of ethylene carbonate (EC)/dimethyl carbonate (DMC) with the volume ratio of 1:1 was taken as an electrolyte and Celgard 2500 was used as a separator membrane. Stationary voltammetry and discharge curves presented in what follows correspond to at least 5th scan.

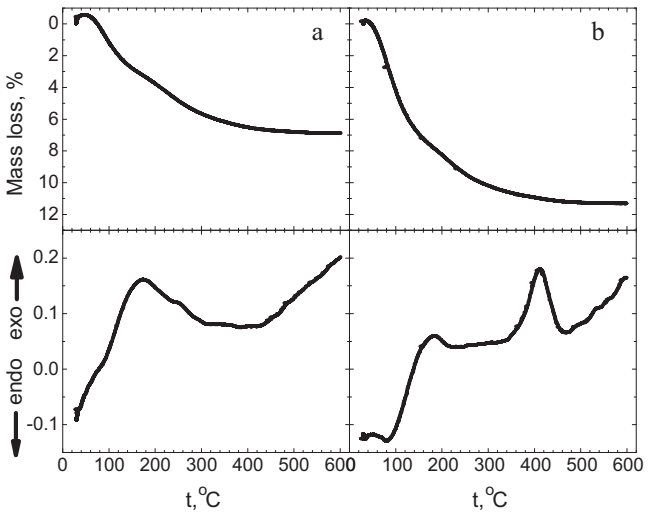

Fig. 1. DTA (above) and TG (below) curves for precursors I (a) and II (b).

3. Results and discussion

Air dry samples contain significant amount of water, which could be removed upon the thermal treatment, i.e. represent hydrous titanium oxide. According to the mass loss data (Fig. 1), precursor I contains less water than precursor II. For both, water loses in two steps ill-recognizable on DTA curves, one at ca. 100 °C and another at ca. 200 °C. At heating speeds typical to thermal analysis studies (5–10 °C min^{-1}), the complete removal of water occurs at around 600 °C. However, water-free crystalline samples could be obtained upon heating air-dry TiO_2 precursor I at 140 °C by several hours.

As follows from DTA curves, precursor I exhibits a broad exothermal effect with a maximum at 150–180 °C, which could be assigned to the crystallization of an initially amorphous substance. In the case of precursor II, DTA curves demonstrate two broad exothermal peaks (Fig. 1b). The first peak has the same shape as in precursor I and probably corresponds to its traces in precursor II. The second peak is more pronounced and corresponds to the crystallization process of the main amount of precursor II.

Conclusions drawn are well supported by X-ray data. Both air dry precursors demonstrate no diffraction peaks. Upon heating at 150 °C, precursor I becomes crystalline (Fig. 2a). Unlike it, precursor II becomes distinctly crystalline just at 470 °C (Fig. 2b). Some peaks discernible at lower temperatures most probably correspond to the beginning of the crystallization process. Changes in crystallite sizes $R_{cryst.}$ in the course of the thermal treatment determined

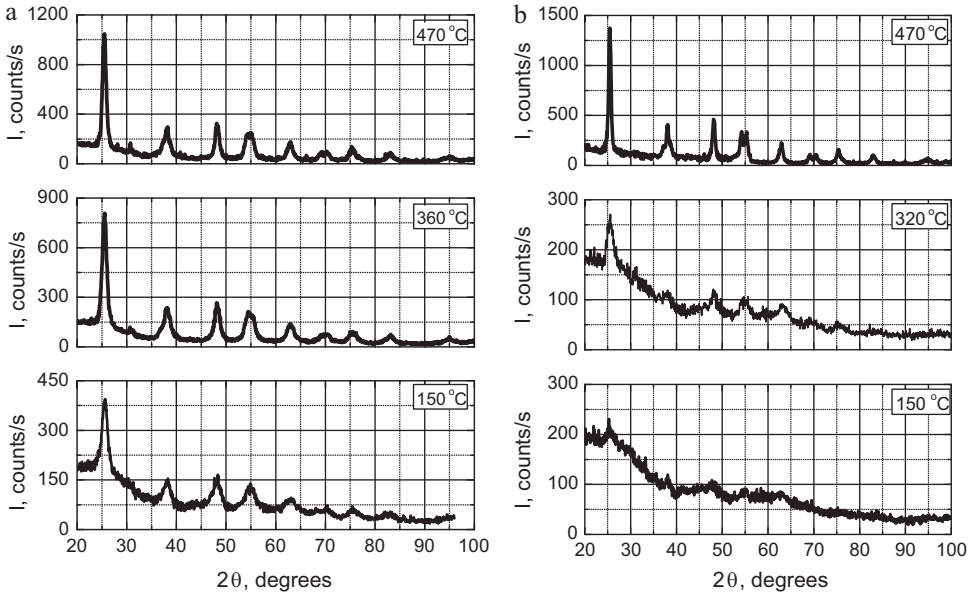

Fig. 2. XRD data for precursors I (a) and II (b). All diffraction peaks correspond to anatase (JCPDS, Card # 21-1272).

by means of the Scherrer equation using the widths of the lines corresponding to the reflections from the (1 0 1) and (2 0 0) planes of the anatase crystal ($\theta \approx 25^\circ$ and 48°, respectively) are summarized in Table 1. As follows from these data, the crystallite size of the materials obtained falls in the nanometer scale.

Some of the samples have been subjected to porosity studies. As follows from the nitrogen absorption–desorption data, materials obtained from each precursor demonstrate similar isotherm profiles, hysteresis loops, and pore radii distributions (Fig. 3). Upon low-temperature heating, TiO_2 samples have high and closely comparable specific surface areas $S_{sp.}$ and pore volumes $V_{p.}$, and their mean pore radii calculated as $R_{pore}(mean) = 2V_{p.}/S_{sp.}$ well agree with the R_{pore} (BJH) values obtained from pore radii distributions found according to the Barrett–Joiner–Halenda procedure (Table 1). Precursors treated at 470 °C have much lower $S_{sp.}$ and $V_{p.}$, and their R_{pore} appear much greater. According to the IUPAC classification (pore radii of 1–25 nm [39]), all the samples studied should be considered mesoporous. However, the samples subjected to heating to lower temperatures are quite close to microporous, having pore radii close to 1 nm.

Using the data obtained in porosity studies, one can calculate the particle radius $R_{part.}$ and packing density ρ based on the theory of gapped gapless packing [40] and compare $R_{part.}$ with the $R_{cryst.}$ found in X-ray measurements. This is especially helpful in the case of materials synthesized from precursors heat-treated at the lowest temperatures. For these materials, due to the low degree of crystallinity, X-ray determinations either appear incomplete or even show no distinct lines. As follows from the theory [40], the packing density varies from 0.39 for loosely packed systems to 0.78 for densely packed systems.

The calculation results are presented in Table 1. For precursor I treated at 150 °C, the particle radius reasonably agrees with the crystallite size determined from X-ray data. For precursor II treated at 180 °C, the data regarding the crystallite size are unavailable due to the poor crystallinity of the sample. Interestingly, the size of particles obtained from both precursors appear almost the same. Moreover, for both low-temperature materials, the packing density is quite low. For samples of both types treated at 470 °C, the particle radii are significantly greater than the crystallite sizes suggesting aggregation due to possible sintering process. Such an idea is supported by the values of packing densities which tend to their maximal values.

Distinct tendency of precursors to aggregation clearly follows from the SEM data. Independent on their pre-history, both precursors are formed by quasi-spherical agglomerates of smaller quasi-spherical particles (Fig. 4).

The structure of these agglomerates is clearly seen in TEM studies (Fig. 5). Both precursors treated at low temperatures are formed by particles of 2–3 nm size. Diffraction patterns prove their amorphous nature. Upon heating to 450–470 °C, crystallization takes

Table 1
Crystallite size and surface properties of thermally treated samples of TiO_2.

t (°C)	$R_{cryst.}$ (1 0 1) (nm)	$R_{cryst.}$ (2 0 0) (nm)	$S_{sp.}$ ($m^2\,g^{-1}$)	V_p ($cm^3\,g^{-1}$)	R_{pore} (mean) (nm)	R_{pore} (BJH) (nm)	$R_{part.}$ (nm)	ρ
Precursor I								
150°	2.90	–	364	0.223	1.22	1.7	2.06	0.53
350° 4h	3.70	3.77	132	0.203	3.07	2.2	5.68	0.55
350° 26h	3.76	3.62						
350° 40h	6.01	5.12						
470° 4h	4.38	4.30	20.9	0.062	5.94	4.8	17.7	0.78
470° 40h	6.50	5.89						
Precursor II								
180°	–	–	391	0.298	1.52	1.9	1.92	0.46
320°	2.47	–						
470°	6.50	6.33	37.0	0.098	5.31	12.0	12.7	0.72
700°	12.99	12.65						

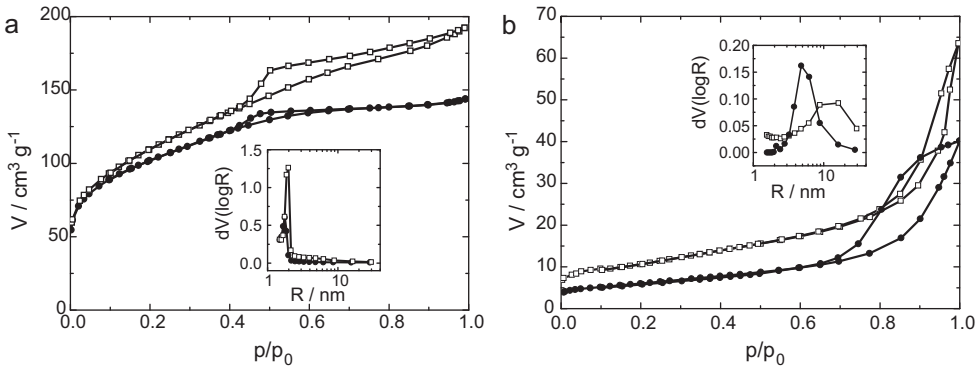

Fig. 3. Nitrogen adsorption-desorption isotherms and pore size distributions (insets) for precursors I (filled circles) and II (empty circles) treated at 150 (a) and 470 °C (b).

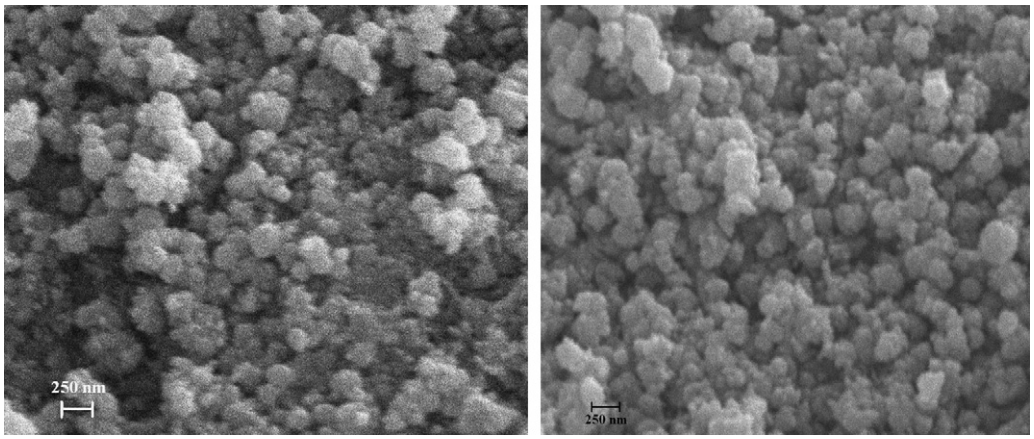

Fig. 4. Scanning electron micrographs (×30,000) for precursors I (left) and II (right) heat treated at 150 °C.

place, and both precursors are comprised of particles of 14–20 nm size. These measurements well agree with the figures obtained in X-ray studies and calculations based on the theory of gapped gapless packing (Table 1).

Summarizing these results (Fig. 6), one can draw the following conclusion regarding materials obtained from precursor I. Heat treatment of precursor I leads to the formation of the crystalline material at temperatures of ca. 350 °C. Once the crystalline material is formed, fast aggregation of crystallites occurs on further heating, best seen in fast decrease in the pore volume and the growth of pore radii R_{pore}, (aggregated) particle radii $R_{part.}$, and packing density ρ. This aggregation whose speed is clearly greater than the growth of the size of crystallites, cf. Fig. 6a and e, leads to worsening electrochemical parameters of TiO_2 in electrode applications (see below). As far as materials obtained from precursor II are concerned, electrochemical studies (see below) reveal that the complete transformation of the amorphous phase to the crystalline phase appears impossible.

Electrochemical testing also proves that materials obtained from precursors I and II behave in a different way. As follows from stationary cyclic voltammetry curves (Fig. 7), TiO_2 obtained from precursor I is clearly crystalline and demonstrates typical peaks corresponding to intercalation and deintercalation of lithium [2–11]. Unlike these materials, TiO_2 obtained from precursor II shows a smooth cyclic voltammetry curve with small traces of intercalation and deintercalation peaks. This so-called capacity behavior [10,41] is characteristic to partly amorphous samples.

As a result, galvanostatic discharge curves for such samples are also unlike (Fig. 8). Crystalline TiO_2 obtained from precursor I at the optimal heat treatment temperature, 350 °C, demonstrates a volt-

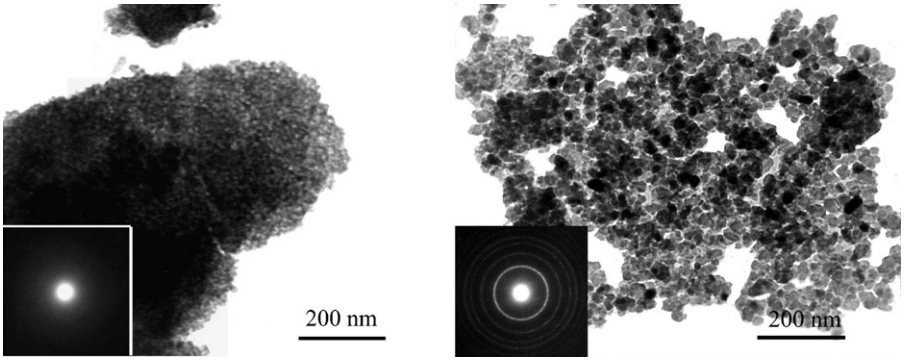

Fig. 5. Transmission electron micrographs (×70,000) for precursor II heat treated at 150 (left) and 470 °C (right). Insets are respective diffraction patterns.

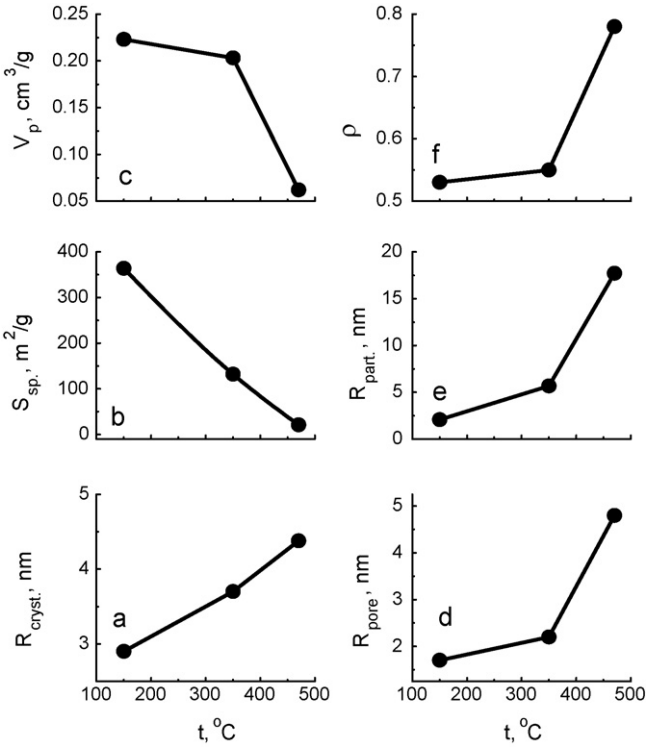

Fig. 6. Temperature dependence of crystallite size and surface properties of thermally treated samples of TiO_2 obtained from precursor I.

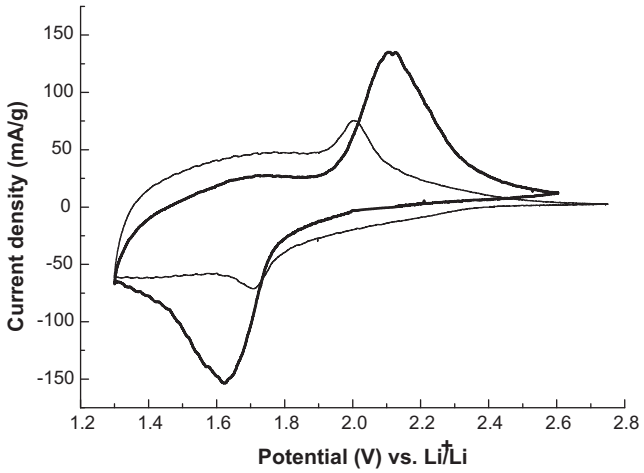

Fig. 7. Stationary cyclic voltammetry curves of TiO_2 obtained by the heat treatment of precursor I at 350 °C (thick line) and TiO_2 obtained by the heat treatment of precursor II at 350 °C (thin line). The scanning voltage rate is equal to 0.1 mV s^{-1}.

age plateau at ca. 1.8–1.6 V and specific capacity of 136 mAh g^{-1}. The dependence of specific capacity of TiO_2 treated at various temperatures on the number of cycle at galvanostatic cycling (Fig. 8, inset a) supports this choice.

On the other hand, TiO_2 obtained from precursor II and treated at a low temperature shows no voltage plateau and has specific capacity of 86 mAh g^{-1} (Fig. 8). Heat treatment at higher temperature leads to the development of a voltage plateau, but the value of specific capacity remains too low (116 mAh g^{-1}, see Fig. 8) due to the presence of remnants of the amorphous structure clearly seen in cyclic voltammetry studies.

Furthermore, galvanostatic studies reveal that the crystalline samples obtained from precursor I are prospective for high rate applications. As an example, in Fig. 8, inset b, the dependence of specific capacity of TiO_2 electrode on the discharge current is shown. It reaches the value of 3350 mA g^{-1} in the continuous discharge mode.

A more detailed description of the electrochemical behavior of crystalline and amorphous varieties of TiO_2 samples obtained by means of the hydrolysis of $TiCl_4$ will be published elsewhere.

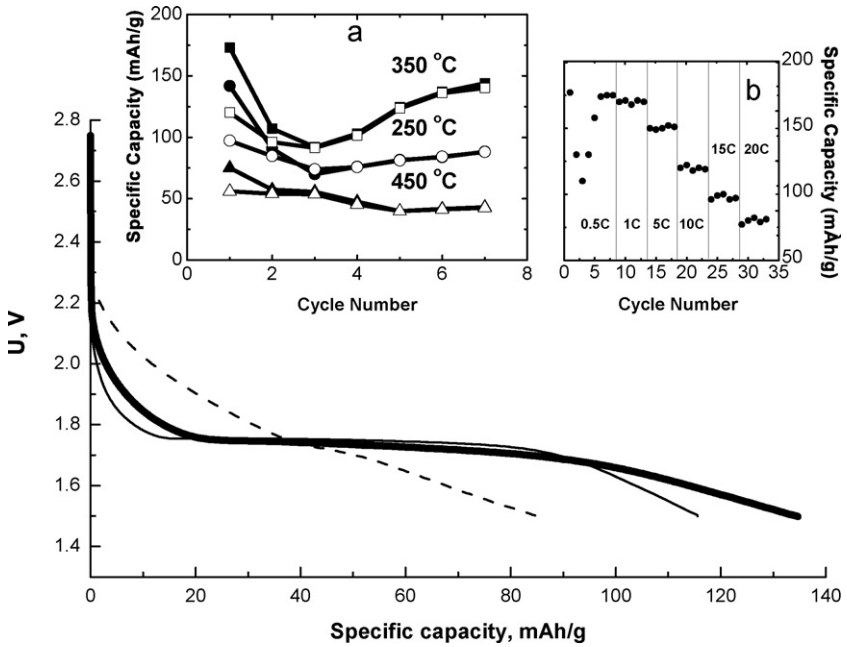

Fig. 8. Stationary discharge curves of TiO_2 obtained by the heat treatment of precursor I at 350 °C (thick line) and TiO_2 obtained by the heat treatment of precursor II at 350 °C (thin dashed line) and at 470 °C (thin solid line). I = 0.5 C. Inset a shows the dependence of specific capacity of TiO_2 (precursor I) treated at various temperatures on the number of cycle at galvanostatic cycling. Circles, 250 °C; squares, 350 °C; triangles, 450 °C. Filled symbols: intercalation, I = 0.5 C, charge cutoff voltage 1.5 V; empty symbols: deintercalation, I = 0.5 C, charge cutoff voltage 2.75 V. The lines are guides for eyes. Inset b demonstrates the dependence of specific capacity of TiO_2 electrode (precursor I, 350 °C) on the discharge current.

4. Conclusions

Summarizing these results one can conclude that in the air-dry state, both TiO_2 precursors obtained by means of precipitation represent hydrous titanium oxide. In spite of the fact that both precursors at low temperatures are, at least, X-ray amorphous, their further evolution is clearly different. On heating, precursor I obtained by means of neutralization of titanium chloride with a metal hydroxide solution gives a nanosized crystalline product at temperatures higher than 140 °C, whereas precursor II synthesized by means of adding $TiCl_4$ to a metal hydroxide solution forms an amorphous product, which cannot be crystallized at temperatures lower than 450 °C. Both materials tend to aggregate upon heating. Aggregation leads to significant compaction of samples, shrinks their surface area and decreases porosity, but crystallites that form aggregates remain of nanometer size.

Differences in the properties of the precursors could be understood in terms of colloid chemistry. The order of mixing leads to significant differences in the composition and structure of micelles and precipitates [42]. Adding a solution of metal hydroxide to the acidic solution of $TiCl_4$ one ensures the complete neutralization of hydroxide ions but cannot substitute Cl^- ions completely. Micelles of the following composition, $\{[m\mathrm{TiO(OH)_2}]n\mathrm{TiO^{2+}}2(n-x)\mathrm{Cl^-}\}^{2x+}2x\mathrm{Cl^-}$, are forming, then adjoining and precipitating. Treating the precipitate with water leads to the substitution of Cl^- ions by OH^- ions, $\{[m\mathrm{TiO(OH)_2}]n\mathrm{TiO^{2+}}2(n-x)\mathrm{OH^-}\}^{2x+}2x\mathrm{OH^-}$, and to further transformation of the precipitate to hydrous titanium oxide, $\{[m\mathrm{TiO(OH)_2}](n-x)\mathrm{TiO(OH)_2}x\mathrm{TiO^{2+}}\}^{2x+}2x\mathrm{OH^-}$.

Adding an acidic solution of $TiCl_4$ to the solution of metal hydroxide leads to the complete substitution of chloride ions by hydroxyls and incomplete neutralization of hydroxide. Therefore micelles of the following composition, $\{[m\mathrm{TiO(OH)_2}]n\mathrm{OH^-}(n-x)\mathrm{M^+}\}^{-x}x\mathrm{M^+}$, are forming, adjoining and precipitating. Treating the precipitate with water leads to the substitution of M^+ ions by H^+ ions: $\{[m\mathrm{TiO(OH)_2}]n\mathrm{OH^-}(n-x)\mathrm{H^+}\}^{-x}x\mathrm{H^+}$. The titanium ions in the latter precipitate should be packed less regularly than in the former one. This means that depending on the order of mixing one gets precursors of crystalline (the former scheme, precursor I) and amorphous (the latter scheme, precursor II) oxides.

Heat treatment of precursor I leads to the formation of the crystalline material at temperatures of ca. 350 °C. Once the crystalline material is formed, fast aggregation of crystallites occurs on further heating, best seen in fast decrease in the pore volume and the growth of pore radii, particle radii, and packing density. Such aggregation process is faster than the growth of the size of crystallites and leads to worsening electrochemical parameters of TiO_2 in electrode applications. Heat treatment of precursor II does not allow for the complete transformation of the amorphous phase to the crystalline phase.

Electrochemical studies demonstrate that nanosized crystalline TiO_2 obtained from precursor I at the optimal heat treatment temperature, 350 °C, has a voltage plateau at ca. 1.8–1.6 V and specific capacity of 136 mAh g^{-1}. In lithium-ion 2016 sample cells, it enables one to yield specific currents up to 3350 mA g^{-1}. On the other hand, the thermal treatment of initially amorphous materials (precursor II) does not lead to complete crystallization, and the presence of amorphous TiO_2 is well seen as the so-called capacity behavior of cyclic voltammetry curves. A more detailed description of the electrochemical behavior of these varieties of TiO_2, both crystalline and amorphous, obtained by means of the hydrolysis of $TiCl_4$ will be published in subsequent papers.

References

[1] U. Diebold, Surf. Sci. Rep. 48 (2003) 53–229.
[2] T. Ohzuku, Z. Takehara, S. Yoshizawa, Electrochim. Acta 24 (1979) 219–222.
[3] F. Bonino, L. Busani, M. Lazzari, M. Manstretta, B. Rivolta, B. Scrosati, J. Power Sources 6 (1981) 261–270.
[4] T. Ohzuku, T. Kodama, T. Hirai, J. Power Sources 14 (1985) 153–166.
[5] B. Zachau-Christiansen, K. West, T. Jacobsen, S. Atlung, Solid State Ionics 28/30 (1988) 1176–1182.
[6] L. Kavan, K. Kratochvilová, M. Grätzel, J. Electroanal. Chem. 394 (1995) 93–102.
[7] S.Y. Huang, G. Campet, N. Treuil, J. Porter, K. Chhor, Active Passive Electron. Comp. 19 (1996) 189–198.
[8] P. Krtil, L. Kavan, D. Fattakhova, J. Solid State Electrochem. 1 (1997) 83–87.
[9] I. Exnar, L. Kavan, S.Y. Huang, M. Grätzel, J. Power Sources 68 (1997) 720–722.
[10] P. Krtil, D. Fattakhova, J. Electrochem. Soc. 148 (2001) A1045–A1050.
[11] Z. Yang, D. Choi, S. Kerisit, K.M. Rosso, D. Wang, J. Zhang, G. Graff, J. Liu, J. Power Sources 192 (2009) 588–598.
[12] M.R. Ranade, A. Navrotsky, H.Z. Zhang, J.F. Banfield, S.H. Elder, A. Zaban, P.H. Borse, S.K. Kulkarni, G.S. Doran, H.J. Whitfield, Proc. Natl. Acad. Sci. 99 (2002) 6476–6481.
[13] A.A. Levchenko, G. Li, J. Boerio-Goates, B.F. Woodfield, A. Navrotsky, Chem. Mater. 18 (2006) 6324–6332.
[14] G. Nuspl, K. Yoshizawa, T. Yamabe, J. Mater. Chem. 7 (1997) 2529–2536.
[15] M. Wagemaker, W.J.H. Borghols, F.M. Mulder, J. Am. Chem. Soc. 129 (2007) 4323–4327.
[16] L.J. Hardwick, M. Holzapfel, P. Novák, L. Dupont, E. Baudrin, Electrochim. Acta 52 (2007) 5357–5367.
[17] M.V. Koudriachova, N.M. Harrison, J. Mater. Chem. 16 (2006) 1973–1977.
[18] M. Smirnov, R. Baddour-Hadjean, J. Chem. Phys. 121 (2004) 2348–2355.
[19] A.S. Aricò, P. Bruce, B. Scrosati, J.-M. Tarascon, W. van Schalkwijk, Nat. Mater. 4 (2005) 366–377.
[20] J. Moskon, R. Dominko, R. Cerc-Korosec, M. Gaberscek, J. Jamnik, J. Power Sources 174 (2007) 683–688.
[21] V. Subramanian, A. Karki, K.I. Gnanasekar, F.P. Eddy, B. Rambabu, J. Power Sources 159 (2006) 186–192.
[22] J. Wang, Y. Bai, M. Wu, J. Yin, W.F. Zhang, J. Power Sources 191 (2009) 614–618.
[23] Y. Zhang, H. Zheng, G. Liu, V. Battaglia, Electrochim. Acta 54 (2009) 4079–4083.
[24] Y. Wang, M. Wu, W.F. Zhang, Electrochim. Acta 53 (2008) 7863–7868.
[25] J. Xu, Y. Wang, Z. Li, W.F. Zhang, J. Power Sources 175 (2008) 903–908.
[26] J. Xu, C. Jia, B. Cao, W.F. Zhang, Electrochim. Acta 52 (2007) 8044–8047.
[27] B. Erjavec, R. Dominko, P. Umek, S. Sturm, A. Pintar, M. Gaberscek, J. Power Sources 189 (2009) 869–874.
[28] H.-G. Jung, S.W. Oh, J. Ce, N. Jayaprakash, Y.-K. Sun, Electrochem. Commun. 11 (2009) 756–759.
[29] L. Kavan, J. Rathouský, M. Grätzel, V. Shklover, A. Zukal, J. Phys. Chem. B 104 (2000) 12012–12020.
[30] H. Yamada, T. Yamato, I. Moriguchi, T. Kudo, Chem. Lett. 33 (2004) 1548–1549.
[31] J. Yan, H. Song, S. Yang, J. Yan, X. Chen, Electrochim. Acta 53 (2008) 6351–6355.
[32] H. Qiao, L. Xiao, L. Zhang, Electrochem. Commun. 10 (2008) 616–620.
[33] M. Mancini, P. Kubiak, J. Geserick, R. Marassi, N. Hüsing, M. Wohlfahrt-Mehrens, J. Power Sources 189 (2009) 585–589.
[34] A. Attia, M. Zukalova, J. Rathouský, A. Zukal, L. Kavan, J. Solid State Electrochem. 9 (2005) 138–145.
[35] C. Challener, Chem. Market Rep. 263 (2003) #18.
[36] O.I. Pendelyuk, T.V. Lisnycha, V.V. Strelko, S.A. Kirillov, Adsorption 11 (2005) 799–804.
[37] S.A. Kirillov, T.V. Lisnycha, O.I. Pendelyuk, Sep. Sci. Technol. 24 (2006) 895–906.
[38] T.V. Lisnycha, V.S. Aleksandrova, O.P. Zykova, T.A. Khodakovskaya, S.A. Khainakov, J.R. Garcia, S.A. Kirillov, J. Appl. Chem. (Russ.) 82 (2009) 951–955.
[39] K.S.W. Sing, D.H. Everett, R.A.W. Haul, L. Moscow, R.A. Pierotti, J. Roquerol, T. Siemieniewska, Pure Appl. Chem. 57 (1985) 603–619.
[40] S.A. Kirillov, Microporous Mesoporous Mater. 122 (2009) 234–239.
[41] A. Attia, M. Zukalová, J. Rathouský, A. Zukal, L. Kavan, J. Solid State Electrochem. 9 (2005) 138–145.
[42] E.A. Hauser, Chem. Rev. 37 (1945) 287–321.